Synthesis of Amid-MCM-41-SO3H Electrospun Nanofiber Mat: Candidate for Trapping of Microorganisms

Mostafa Golshekan (mostafa.golshekan@gmail.com)
Guilan University of Medical Sciences
Hossein Hemmati
Guilan University of Medical Sciences
Mohammad Taghi Ashoobi
Guilan University of Medical Sciences
Khatereh Asadi
Guilan University of Medical Sciences

Research Article

Keywords: microorganisms, Nano filter, Electrospinning, Amid-MCM-41-SO3H

Posted Date: May 11th, 2021

DOI: https://doi.org/10.21203/rs.3.rs-370532/v1

Abstract

In the present study, amid-MCM-41-SO_3H nano-composite is fabricated through the electrospinning process, which will a significant step toward air filtration for removal of microrganism from air particularly ICU hospital. The filtration mechanism of the amid-MCM-41-SO_3H composite is based on the interaction of nanofiber functionalized group (-SO_3H) with surface active groups of lipids and protein of microorganisms such as SARS-CoV-2. For the characterization of the synthesized nano-composite, various instrumentation methods were used. the SEM and TEM showed that the MCM-41- SO_3H nanoparticles were uniformly distributed throughout the fiber length. Fourier Transform Infrared (FT-IR) spectroscopy confirms with the synthesized Amid-MCM-41-SO_3H filter. X-ray Diffractometry (XRD) pattern indicated that the structure of the MCM-41-SO_3H composite was well-preserved after modification. These results suggested that the amid-MCM-41-SO_3H composite has higher performance in interaction with similar NPs of virus.

1- Introduction

The severe acute respiratory syndrome coronavirus 2 (SARS-CoV-2) is conducted for the emergence of the COVID-19 pandemic in Wuhan, China, which the initial symptoms of disease were warned in February 2019. To date, more than 16 million cases have been reported in 210 countries, of which 650,000 have died.

SARS-CoV-2 is a 60–140 nm spherical particle, with a crown-like shape glycoprotein coating. It belongs to the subgenus Sarbecovirus and genus Betacoronavirus within the family Coronaviridae [1].

SARS-CoV-2 is an enveloped virus with a very large positive-strand RNA genome, compromised of ~ 3 k nucleotides. Virus RNA polymerases have poor proofreading activity, leading to a high mutation rate. Consequently, RNA viruses are prone to evolving resistance to drugs and escaping from immune surveillance [2].

The coronaviral genome encodes four major structural proteins: the spike (S) protein, nucleocapsid (N) protein, membrane (M) protein, and the envelope (E) protein. The envelope bears club-shaped glycoprotein projections. Some coronaviruses also contain a hem agglutinin-esterase protein (HE). The lectin domain of HE protein helps attachment of virus-host cells, thus playing a key role in the production of infectious virions and the severity of the disease [3, 4].

CoV S protein is one of the key components in receptor binding and virus-host cell fusion, and it is also the main target for neutralizing antibodies and vaccine design [5–10]. The CoV E protein is a small integral membrane protein that involved in virus vital activity as assembly, budding, envelope formation, and pathogenesis. Studies have shown that SARS-CoV E protein is an important virulence factor that can contribute to therapeutic targets [11].

SARS-CoV-2 exhibits a high mutation rate during its interaction with the host population and transmission across the countries that are affected by its viral infections and high mortality rate. Recent studies have reported more than 40 mutations of SARS-CoV2 virus, and the strains grouped into aggressive form and milder types [12–15]. But different types of CoVs have highly similar surface chemical structures. The surface of the virus consists of the elements oxygen, sulfur, hydrogen and etc, that can also form strong bonds with other functional groups [16, 17].

The SARS-CoV-2 can attach to the human secretion that spread through air droplets and airborne. Infected people could expel pathogens during breathing, coughing, sneezing, and medical procedures which remain suspended particles in the air [18]. Several factors may affect the droplet dispersion including the relative humidity, ventilation pattern, temperature, crowding and other environmental factors. Hospitals particularly intensive care units (ICU) or wards for COVID 19 patients need to critically improve their safety practices especially for medical staff [19, 20].

One of the most important ways to deal with microorganisms (SARS-CoV-19) is to take a commercial breathing mask to prevent the inhalation of airbornes, when going outdoors or staying indoors especially in the hospital, air quality is ensured by employing the air cleaners or modern ventilation systems. In general, the dimensions of aerosolized virus particles vary widely, ranging from nanometer to micrometer [21]. It is very difficult to reduce air pollution problems, especially nanometer particles. Besides the complexity of the conventional air filter that mainly constitue of several layers of randomly oriented melt-blown micron-scale fibers showed unsatisfied yield. Conventional filter have sevral inherent functional obstacles of capturing fine particles [22]. Electrospun nanofibers provided highly efficient, interconnected nanoscale pore structures and biocompatible nanofibrous filters for air purification. Nanofibrous filters based on their high porosity (physical barrier) and surface modification technologies (chemical barrier) could be a good choice for viral filtration [23].

Here, we present the synthesis of nanofiber of amid-MCM-41-SO_3H via the electrospinning process, which will a significant step toward air filtration particularly hospital. In the process of air purification using the proposed filter, to ensure the removal of the virus from the air, in addition to creating a mechanical barrier (Amid nanofiber), a chemical barrier is embedded in this filter (MCM-41-SO_3H) [24], which can be bond formed with functional groups on the virus surface (Fig. 1).

2- Experimental

2-1-Materials and Apparatus

All chemicals including 3-mercaptopropyl Triethoxysilane (MPTMS), acetic acid (99%), Cetyltriammonium bromide (CTAB), tetraethyl orthosilicate (TEOS), NaOH, NaF, Poly-amide 6 pellets, as well as formic acid (85%), dichloromethane (98%) and hydrogen peroxide were purchased from Fluka (Chemie AG, Switzerland) and Merck (Darmstadt, Germany). The crystal phases and crystallinity of synthesized MCM-41-SO_3H were characterized by X'PERT PRO X-ray diffraction (PANalitical) and measured with Cu–Ka

radiations in the 2θ range of 0-10. were characterized by a the Shimadzu Fourier transform infrared (FT-IR-470) was used for quality and composition of synthesized composite. The PHILIPS transmission electron microscopy (TEM, CM10 HT 100KV) was used for study of size and morphology of synthesized composite.

2-2-Preparation of MCM-41–SO_3H nano-composite

According to our previous work [25-27], for the synthesis of MCM-41–SO_3H, tetraethyl orthosilicate (TEOS) (7.0 mL), 3-mercapto propyl Triethoxysilane (MPTMS) (5.0 mL), NaOH (0.9 g) and NaF (0.19) were used. The Cetyltrimethylammonium bromide (CTAB) (8.0 g) was used as template and And removed at the end of the synthesis process by solvent extraction. Finally, the thiol group was oxidated to the sulfonic acid.

2-3-Preparation of nanofiber of amid-MCM-41-SO_3H

For the preparation of a homogeneous solution, 25% (w/vol) PA was dissolved in a solution of formic acid/acetic acid (FA/AA) 3 : 2 ratio (vol/vol). Then 1000 mg/L of MCM-41-SO_3H nano-composite was slowly added to the solution while the solution was stirring. Finally, the solution was sonicated for 30 min.

A electrospinning device with four-needle system was used in electrospinning experiments. This device consisted of a high voltage DC power supply based on the flyback principle. To start electrospinning, the high voltage electrode was connected to the needles of the syringe and the grounded electrode was connected to the collector. The PA solutions were loaded into a syringe equipped with four needle. Electrospun fibers were collected on an activated filter paper (EASTAR Thickness 0.35-0.70 mm) vertically positioned cylindrical collector and rotating at a linear speed of 20 cm/min. The electrospinning process parameters were as follows: voltage of 14 and 18 kV, a feed rate of 1.0 mL/h, and tip-to-paper distance of 6 cm. The electrospinning process parameters for PA 6 were voltage of 14 and 18 kV.

2-4-Trapping test of synthesized Amid-MCM-41-SO_3H filter

To evaluate the performance of the amid-MCM-41-SO_3H filter in trapping of particles similar to the virus: (I) Triglyceride and glycerol-functionalized iron magnetite nano-composites (TGI NPs) with dimensions of 20-50 nm were synthesized, then dispersed in water, (II) The solution containing triglyceride and glycerol-functionalized nano-composites (200 mL with 100 μg L^{-1} concentration from each composite) was adjusted to the appropriate pH (pH 7.0), (III) Finally, the prepared solution was passed through the filter and the amount of composites were investigated in solution. After extraction of triglyceride and glycerol

from the magnetic nano-composites, the gas chromatography used for the analysis of triglyceride and glycerol concentration.

2-5-GC Analysis of TGI NPs: extraction and sample preparation

For the extraction of TGI NPs from water solution, 50 mL of solution (after filtration) was used. 5 mL n-Hexane as extract solvent in 5 mL acetonitrile as dispersive solvent was rapidly injected into the sample solution using a 10 mL syringe and then mixed at room temperature for 40 s. Subsequently, using a Nd-Fe-B strong magnet the Fe_3O_4 nano-particles were isolated from the solution . Finally, the extracted solution was injected directly into the GC. The separation was achieved on a capillary column (RTX 65-TG). The injector temperature was programmed as follows: 50°C was maintained for 15 sec, followed by an increase at 900°C/min to 390°C and a 7 min hold. The oven temperature was programmed as follows: 250°C was maintained for 2 min, followed by an increase at 5°C/min to 360°C and a 4 min hold. The detector temperature was 370°C. Hydrogen was used as the carrier gas at a flow rate of 1.5 mL/min.

3- Results And Discussion

In the present study, a new and effective Amid-MCM-41-SO_3H nanofiber proposed for filtering COVID 19 (Fig. 2). This nano-composite design based on fabricating an amid nanofiber (mechanical barrier) and passive targeting principles (-SO_3H modifications). It is expected to be an *effective* viral filter due to the mutation pattern of SARS COV 2 [28]. Surfaces of our fabricated filter saturated with SO_3H functional groups that constituted a strong bond with -COOH, -PO_4^{3-} -NH, and -OH functional groups exit on lipid enveloped of SARS-CoV-2 (Chemical barrier). Therefore, sulfhydryl (R-S-H) formation plays an important role in the absorption of viruses from airbornes. In addition, surface modification of fabricated filter with –SO_3H groups could be a proper target for amine and phosphate groups of spike protein [29-32]. These strategies improve the efficiency of current air ventilation. Amid-MCM-41-SO_3H nanofiber filter fabrication process involves (i) synthesis of functionalized amid nanofiber by MCM-41-SO_3H nanofiber (ii), Optimization of variables (iii), Characterization of the synthesized filter.

3-1-Characterization of the Synthesized Amid-MCM-41-SO_3H filter

The Amid-MCM-41-SO_3H filter was evaluated via FT-IR, XRD, SEM and TEM.

Figure 3 display the FT-IR spectra of MCM 41 (a) and MCM 41-SO_3H (b). The FT-IR analysis that confirms the synthesized Amid-MCM-41 filter.

Raman spectroscopy could also confirm the existence of –SH, which is around 2550 to 2600 cm^{-1}. The vital peak which could confirm the existence of thiol groups. There is a strong and sharp peak at 1270 cm−1 which is an indication of CH_3-Si(−O)$_3$ conveying the successful modification of MCM-41. Moreover, a strong band at 1174 cm-1 is assigned to the Si–O– Si asymmetric stretching vibrations and a band at 850 cm-1 related to its symmetric stretching vibrations, respectively. There are hydroxyl groups on the surface as indicated with strong peaks around 3200 and 3400 cm. The existence of OH groups on the mesoporous material surface after the sulfonation[33].

The structure of amid-MCM-41-SO_3H nanofiber was characterized by XRD and the results are shown in figure 4. MCM-41 displayed a well-resolved reflection of the 2D-hexagonal structure at (100), (110), and (200) observed from the small-angle XRD pattern. The diffraction patterns of MCM-41 and PEI-MCM-41 were quite similar, which indicated that the structure of MCM-41 was well preserved after modification. However, the sharp three peaks with 2 at 1.5–10◦ which are characteristic peaks of MCM-41.

The SEM image figure 5A,B showed, the amid nanofiber and the amid-MCM-41-SO_3H nano-scaffold consecutively. Figure 5b shown the MCM-41-SO_3H composite was located in the structure of the amid nanofiber with high-density. To observe the structure of the synthesized amid-MCM-41-SO_3H nanofiber, TEM was used, figure 5C showed the connection bitween MCM-41-SO_3H and amid nanofiber, which confirms the structure of the synthesized nano-composite in the filter. figure 5D showed the MCM-41-SO_3H nano-composite that confirms its porous structure.

The N_2 adsorption-desorption isotherms for the filter are shown in Figure. 6. The adsorption-desorption isotherm in conformity with the IVa type in IUPAC classification which corresponds to mesoporous structures [34].

3-2-Optimization of variables

In the proposed procedure, to achieve maximum extraction efficiency, one parameter affecting the trapping of TGI NPs was optimized. Hence, the effect of pH was studied. All optimizing experiments were done at Falcon tubes with 50 mL volumes, and 100 µg L−1 of TGI NPs were used for optimization.

3-3-Influence of pH

The effect of pH on the process trapping has a profound influence on the adsorptive of TGI NPs because this parameter plays an important role in the surface properties of the filter and bond formation of the filter and TGI NPs. Hence, the effect of pH on the trapping of target composites onto filter was studied at a pH range of 3.0–9.0. As can be seen in Figure. 7, the maximum trapping of target composites occurred at pH ranges of 5.0–7.0 (the TGI NPs concentration at solution was cheked after filtration). Hence, pH 7.0

was chosen as the optimum pH for subsequent experiments in which SO_3H constituted tight bonds with functional groups on the surfaces of synthesized TGI NPs.

4- Conclusion

In the present study, we proposed amid-MCM-41-SO3H nanofibers as a mechanical and chemical barier for air ventilation based on the chemical interaction of SO3H with functional groups on the surfaces of the virus's envelope. Due to SARSCOV 2 wide mutation rate, the nonspecific function of this filter could be the efficient selection for air ventilation in critical wards.

Declarations

Funding

This work did not receive a financial support.

Conflict of Interest

The authors declare that they have no conflict of interest.

Availability of Data and Material

The data and material are available within the manuscript.

Code availability

Not applicable.

Authors' Contributions Conceptualization:

Golshekan M, Hemmati H, Ashoobi MT, Asadi Kh Methodology, Writing - original draft preparation and Formal analysis and investigation: Golshekan M, Hemmati H, Ashoobi MT, Writing – review and editing: Golshekan M, Hemmati H, Ashoobi MT.

Ethics approval

Not applicable.

Consent to Participate

Not applicable.

Consent for Publication

Not applicable.

References

1. Mousavizadeh L, Ghasemi S (2020) Genotype and phenotype of COVID-19: Their roles in pathogenesis, Journal of Microbiology. Immunology and Infection https://doi.org/10.1016/j.jmii.2020.03.022
2. Amanat F, Krammer F (2020) SARS-CoV-2 vaccines: status report,Immunity 52:583-589
3. Schoeman D, Fielding BC (2019) Coronavirus envelope protein: current knowledge. Virology j.16:1-22
4. Alanagreh La, Alzoughool F, Atoum M (2020) The human coronavirus disease COVID-19: its origin, characteristics, and insights into potential drugs and its mechanisms. Pathogens.9:331-236
5. Abdelmageed MI, Abdelmoneim AH, Mustafa MI, Elfadol NM, Murshed NS, Shantier SW, Makhawi AM (2020) Design of a Multiepitope-Based Peptide Vaccine against the E Protein of Human COVID-19: An Immunoinformatics Approach. BioMed Research International doi.org/10.1155/2020/2683286
6. Wang N, Shang J, Jiang S, Du L (2020) Subunit vaccines against emerging pathogenic human coronaviruses. Frontiers in microbiology.11:298-302
7. Rabi FA, Zoubi MS, Kasasbeh GA, Salameh DM, Al-Nasser AD (2020) SARS-CoV-2 and coronavirus disease 2019: what we know so far. Pathogens.9: 231
8. Lu R, Zhao X, Li J, Niu P, Yang B, Wu H, Wang W, Song H, Huang B, Zhu N (2020) Genomic characterisation and epidemiology of 2019 novel coronavirus: implications for virus origins and receptor binding. Lancet 395: 565-574.
9. Ou X, Liu Y, Lei X, Li P, Mi D, Ren L, Guo L, Guo R, Chen T, Hu J (2020) Characterization of spike glycoprotein of SARS-CoV-2 on virus entry and its immune cross-reactivity with SARS-CoV. Nature communications.11:1-12.
10. Zhang J, Zeng H, Gu J, Li H, Zheng L, Zou Q (2020) Progress and prospects on vaccine development against SARS-CoV-2. Vaccines 8: 153-166.
11. Junior IJM, Polveiro RC, Souza GM, Bortolin DI, Sassaki FT, Lima ATM (2020) The global population of SARS-CoV-2 is composed of six major subtypes. BioRxiv, doi: 10.1038/s41598-020-74050-8
12. Wang H, Li X, Li T, Zhang S, Wang L, Wu X, Liu J (2020) The genetic sequence, origin, and diagnosis of SARS-CoV-2. Eur J Clin Microbiol Infect Dis 24: 1–7.

13. Bajaj A, Purohit HJ (2020) Understanding SARS-CoV-2: genetic diversity, transmission and cure in human. Indian Journal of Microbiology 60: 398–401.
14. Zhao Z, Sokhansanj BA, Rosen G (2020) Characterizing geographical and temporal dynamics of novel coronavirus SARS-CoV-2 using informative subtype markers. BioRxiv doi: 10.1371/journal.pcbi.1008269
15. Kim D, Lee JY, Yang JS, Kim JW, Kim VN, Chang H (2020) The architecture of SARS-CoV-2 transcriptome. Cell 181: 914-921
16. Robson B (2020) COVID-19 Coronavirus spike protein analysis for synthetic vaccines, a peptidomimetic antagonist, and therapeutic drugs, and analysis of a proposed achilles' heel conserved region to minimize probability of escape mutations and drug resistance. Computers in Biology and Medicine 121:103749
17. Zhang Y, Geng X, Tan Y, Li Q, Xu C, Xu J, Hao L, Zeng Z, Luo X, Liu F, (2020) New understanding of the damage of SARS-CoV-2 infection outside the respiratory system. Biomedicine & Pharmacotherapy 127:110195.
18. Wang R, Hozumi Y, Yin C, Wei GW (2020) Decoding SARS-CoV-2 transmission, evolution and ramification on COVID-19 diagnosis, vaccine, and medicine. J. Chem. Inf. Model 60:5853–5865
19. Dietz L, Horve PF, Coil DA, Fretz M, Eisen JA, Van Den K (2020) Wymelenberg,2019 novel coronavirus (COVID-19) Pandemic: Built environment considerations to reduce transmission. Msystems DOI: 10.1128/mSystems.00245-20
20. Pan M, Lednicky JA, Wu CY (2019) Collection, particle sizing and detection of airborne viruses. Journal of applied microbiology 127: 1596-1611
21. Zhu M, Han J, Wang F, Shao W, Xiong R, Zhang Q, Pan H, Yang Y, Samal SK, Zhang F (2017) Electrospun nanofibers membranes for effective air filtration. Macromolecular Materials and Engineering 302: 1600353
22. Sundarrajan S, Tan KL, Lim SH, Ramakrishna S (2014) Electrospun nanofibers for air filtration applications. Procedia Eng 75: 159-163.
23. Liverani L, Boccardi E, Beltrán AM, Boccaccini AR (2017) Incorporation of calcium containing mesoporous (MCM-41-type) particles in electrospun PCL fibers by using benign solvents. Polymers 9: 487
24. Saadatjoo N, Golshekan M, Shariati S, Kefayati H, Azizi P (2013) Organic/inorganic MCM-41 magnetite nanocomposite as a solid acid catalyst for synthesis of benzo [α] xanthenone derivatives. J of Molecular Catalysis A: Chemical 377:173-179
25. Golshekan M, Shariati S (2013) Nano magnetic solid phase extraction for preconcentration of lead ions in environmental samples by a newly synthesized reagent. Acta Chimica Slovenica 60:358-367
26. Golshekan M, Shirini F (2020) Fe_3O_4@ MCM-41-(SO^{3-})[ZrO_2] Magnetic Mesoporous Nanocomposite: Dispersive Solid-Liquid Micro Extraction of Pb^{2+} Ions. Silicon 12:747–757

27. Yeo JH, Kim M, Lee H, Cho J, Park J (2020) Facile and Novel Eco-Friendly Poly (Vinyl Alcohol) Nanofilters Using the Photocatalytic Property of Titanium Dioxide. ACS omega 5:5026-5033
28. Podgorski A, Bałazy A, Gradoń L (2006) Application of nanofibers to improve the filtration efficiency of the most penetrating aerosol particles in fibrous filters. Chemical Engineering Science 61: 6804-6815
29. Leung WWF, Chau YT (2019)Experiments on filtering nano-aerosols from vehicular and atmospheric pollutants under dominant diffusion using nanofiber filter. Separation and Purification Technology 213: 186-198
30. Sun Q, Leung WWF (2019) Charged PVDF multi-layer filters with enhanced filtration performance for filtering nano-aerosols. Separation and Purification Technology 212:854-876
31. Leung WWF, Sun Q (2020) Electrostatic charged nanofiber filter for filtering airborne novel coronavirus (COVID-19) and nano-aerosols. Separation and Purification Technology 250:116886
32. Haghighat MF, Shirini F, Golshekan M (2019) Synthesis of Tetrahydrobenzo[b]pyran and Pyrano[2, 3-d]pyrimidinone Derivatives Using Fe□O□@Ph-PMO-NaHSO□ as a New Magnetically Separable Nanocatalyst. Journal of nanoscience and nanotechnology.19: 3447-3458
33. Golshekan M, Shariati S, Saadatjoo N (2014) The synthesis of aminonaphtols and β-amino carbonyls in the presence of a magnetic recyclable Fe_3O_4@MCM-48–$NaHSO_4$ nano catalyst. RSC Advances.4:589-596
34. Thommes M, Kaneko K, Neimark AV, Olivier JP, Rodriguez-Reinoso F, Rouquerol J, Sing KS(2015)Physisorption of gases, with special reference to the evaluation of surface area and pore size distribution (IUPAC Technical Report). Pure and Applied Chemistry 87:1051-1069

Figures

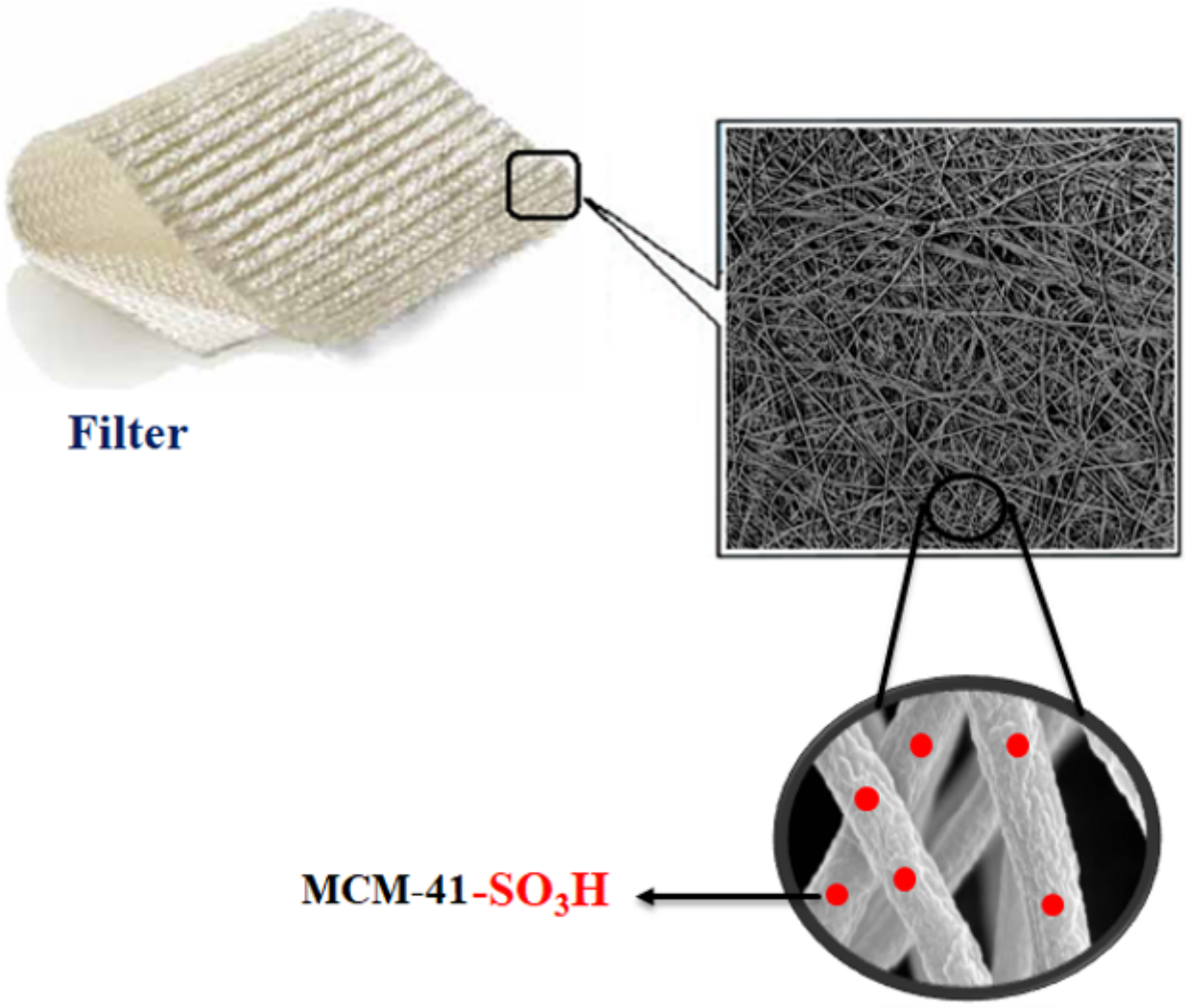

Figure 1

Stracture of amid-MCM-41-SO3H

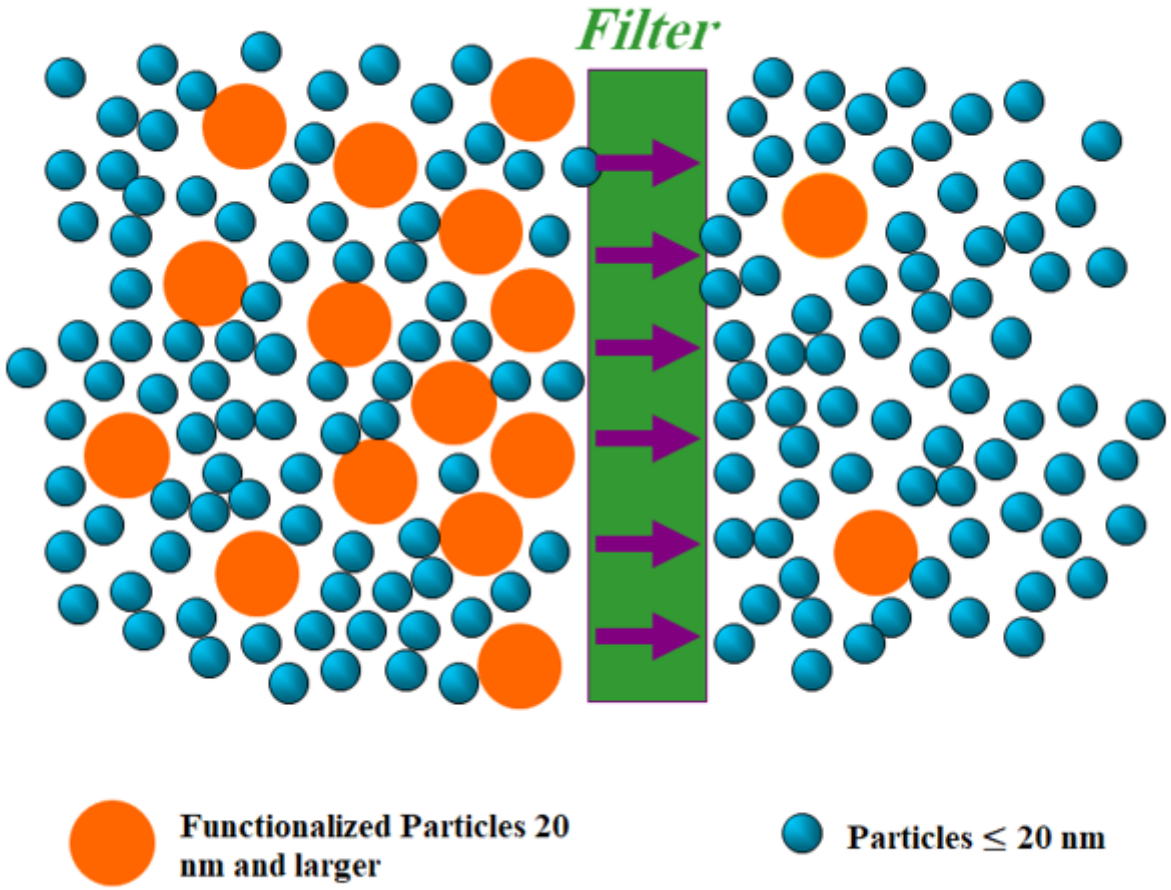

Figure 2

Scheme of synthesized nano filter

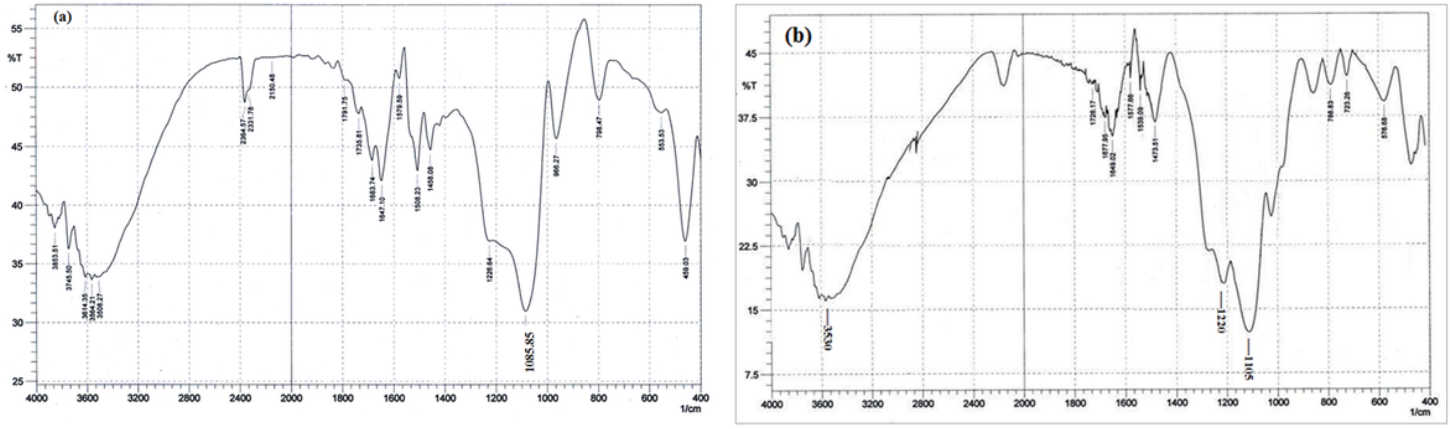

Figure 3

FT-IR spectra of MCM 41 (a) and MCM 41-SO3H (b).

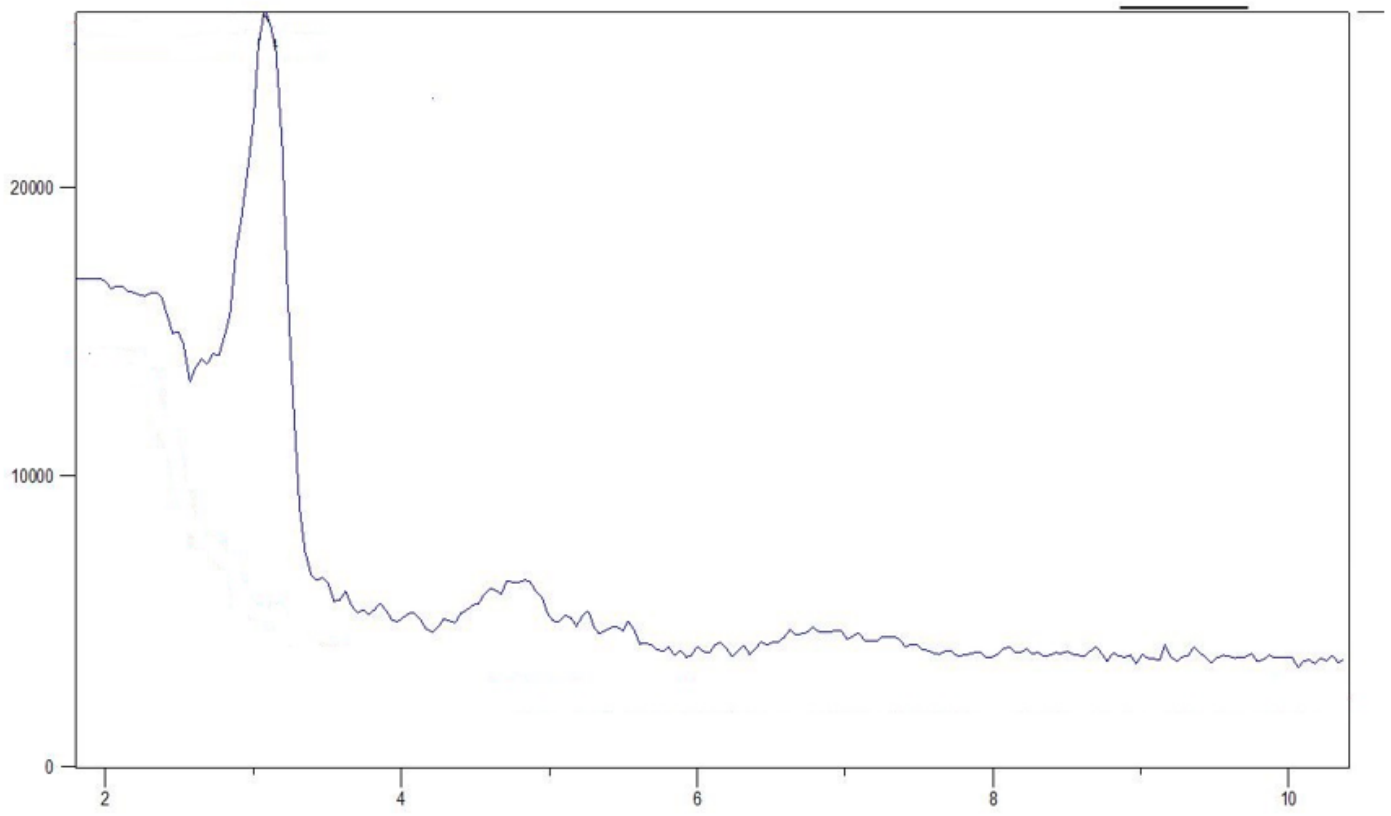

Figure 4

Low-angle powder X-ray diffraction (XRD) of MCM-41-SO3H

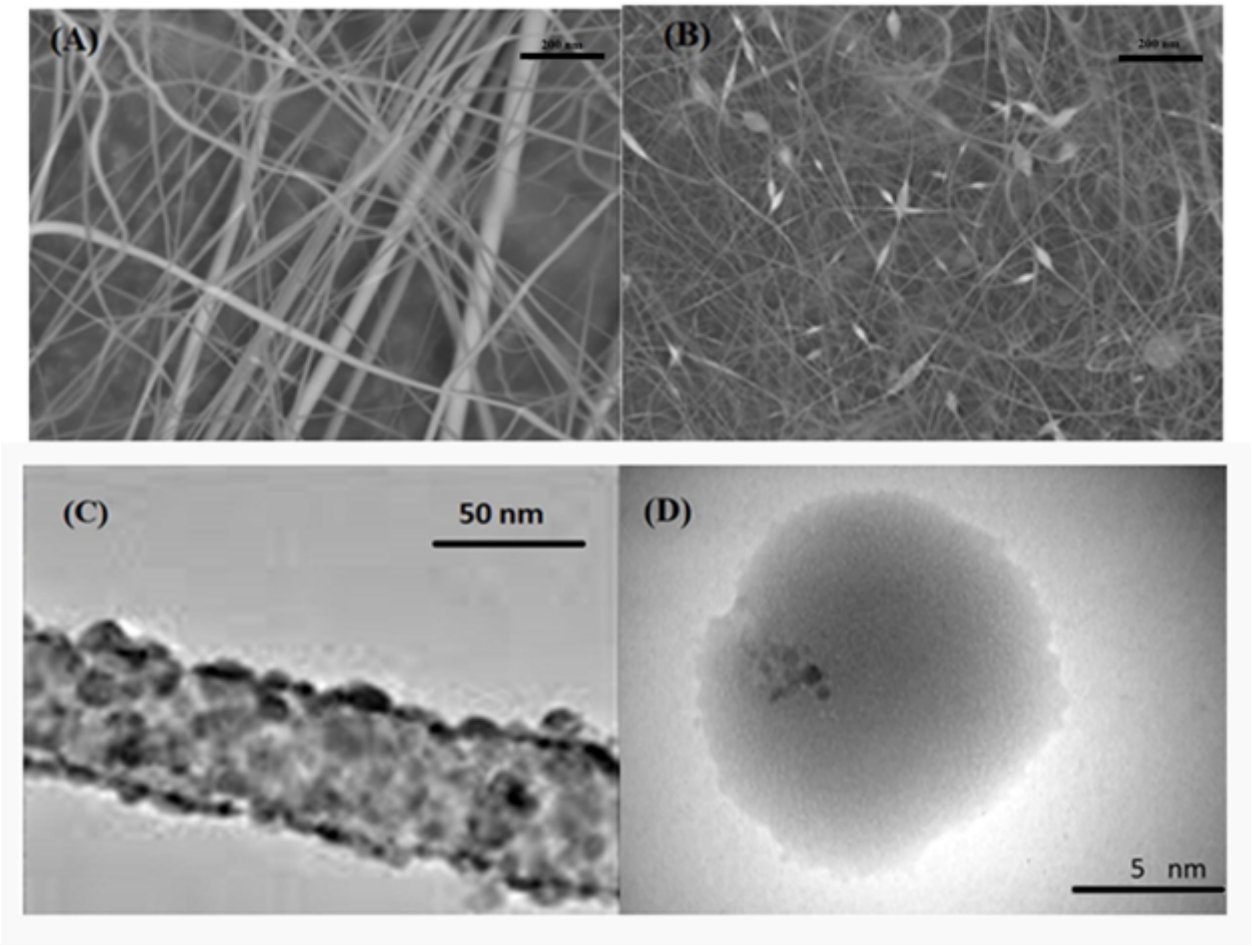

Figure 5

(A) SEM image of Amide nanofiber, (B) SEM image of Amide-MCM-41-SO3H nano-composite, (C) TEM image of Amide-MCM-41-SO3H nano-composite and (D) TEM image of MCM-41-SO3H

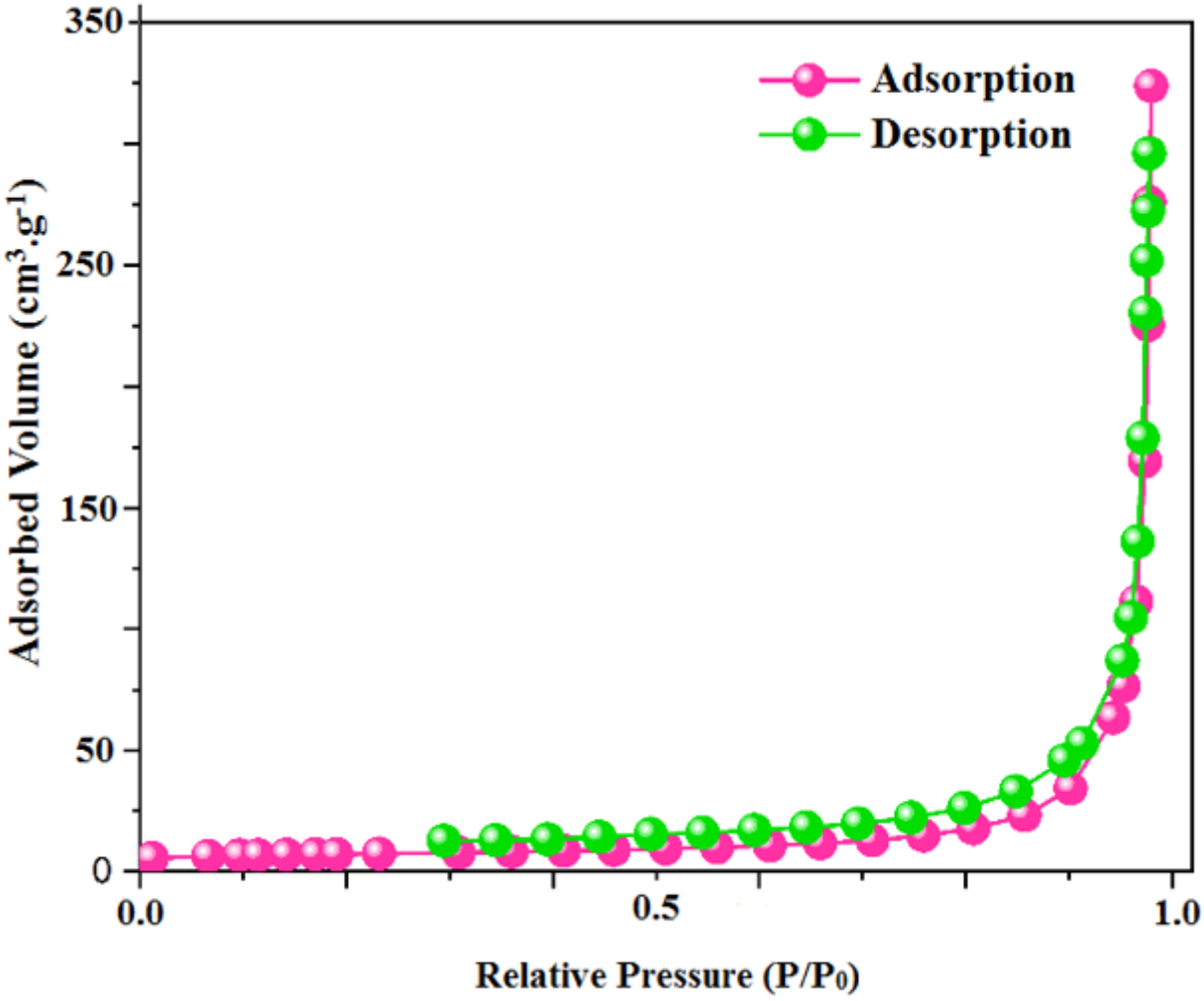

Figure 6

The N2 adsorption-desorption isotherms for the filter

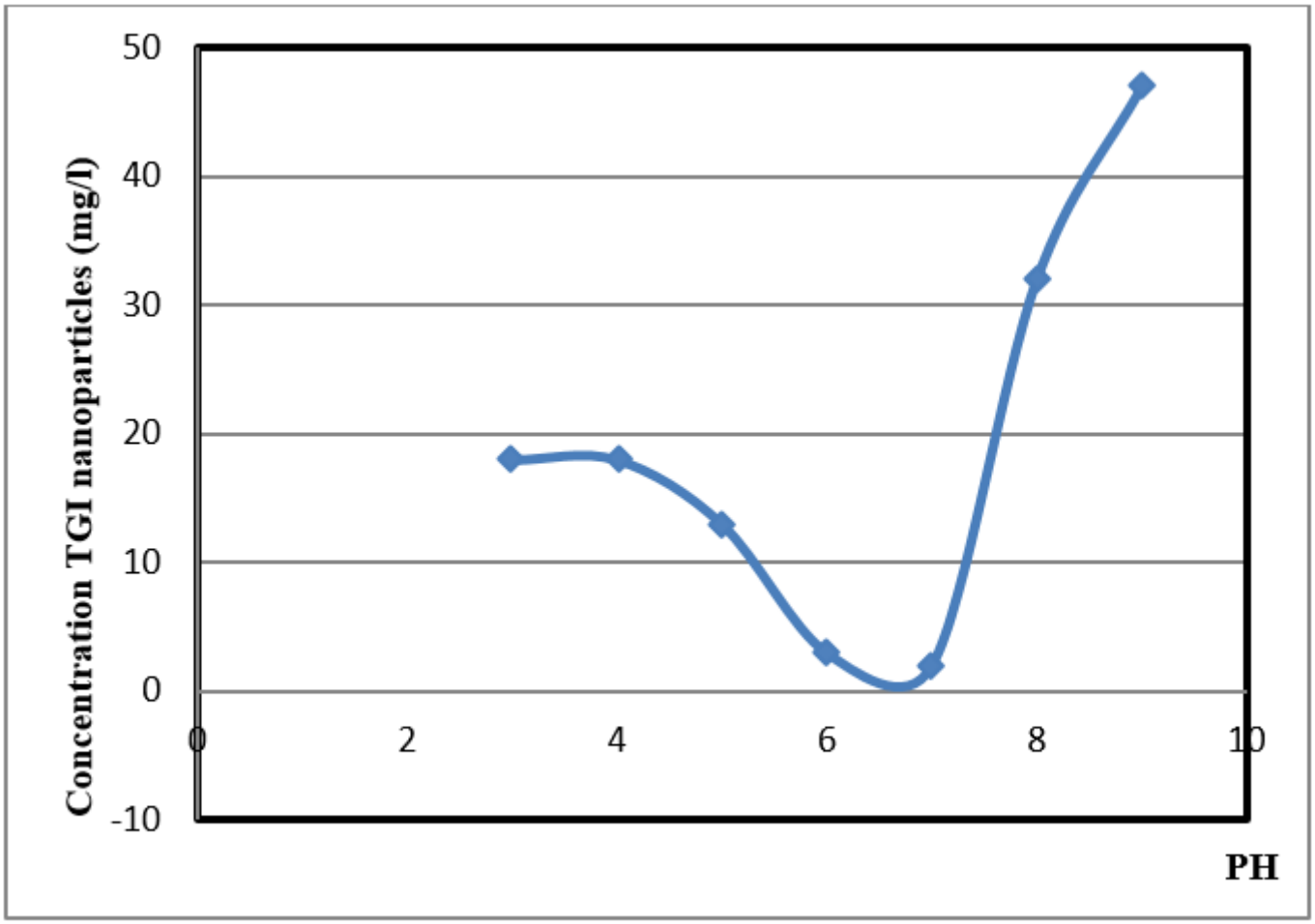

Figure 7

Effect of PH on the trapping of TGI nanoparticles on Amid-MCM-41-SO3H filter